Soft Matter

A simple simulation model for complex coacervates

Journal:	*Soft Matter*
Manuscript ID	SM-ART-06-2021-000881.R1
Article Type:	Paper
Date Submitted by the Author:	25-Aug-2021
Complete List of Authors:	Bobbili, Sai Vineeth; Penn State, Chemical Engineering Milner, Scott; Penn State University,

Soft Matter

ARTICLE TYPE

Cite this: DOI: 00.0000/xxxxxxxxxx

A simple simulation model for complex coacervates

Sai Vineeth Bobbili,[a] and Scott T. Milner*[a]

Received Date
Accepted Date

DOI: 00.0000/xxxxxxxxxx

When oppositely charged polyelectrolytes mix in an aqueous solution, associative phase separation gives rise to coacervates. Experiments reveal the phase diagram for such coacervates, and determine the impact of charge density, chain length and added salt. Simulations often use hybrid MC-MD methods to produce such phase diagrams, in support of experimental observations. We propose an idealized model and a simple simulation technique to investigate coacervate phase behavior. We model coacervate systems by charged bead-spring chains and counterions with short-range repulsions, of size equal to the Bjerrum length. We determine phase behavior by equilibrating a slab of concentrated coacervate with respect to swelling into a dilute phase of counterions. At salt concentrations below the critical point, the counterion concentration in the coacervate and dilute phases are nearly the same. At high salt concentrations, we find a one-phase region. Along the phase boundary, the total concentration of beads in the coacervate phase is nearly constant, corresponding to a "Bjerrum liquid". This result can be extended to experimental phase diagrams by assigning appropriate volumes to monomers and salts.

1 Introduction

Mixing oppositely charged polymers in an aqueous solution results in an associative phase separation with a polymer rich coacervate phase and a dilute phase. In such solutions, the coacervate phase contains both types of polymers, while the coexisting dilute phase contains very low concentrations of each polymer. Such coacervates have wide range of applications including protein encapsulation[1,2], underwater adhesives,[3] and functional materials in the food industry[4,5]. These applications depend on the phase behavior of these complex materials formed using specific oppositely charged polyelectrolytes, understanding of which is critical for optimal design of functional materials[6].

Coacervate solutions exhibit two-phase coexistence, with a phase diagram describing the salt and polymer concentrations in each phase. With addition of salt, the polymer concentration in the complex phase decreases. When enough salt is added, the polymer concentration in both phases is equal, resulting in a single phase. The critical salt concentration is the minimum salt concentration above which we observe no phase separation. This phase behavior is influenced by electrostatic attractions, salt concentration, and to some extent chain length[7–9].

Voorn and Overbeek[10] provided one of the first theoretical descriptions of complex coacervation. They argued that the salt concentration in the coacervate phase must be greater than in the dilute phase, because salt ions will have a lower electrostatic free energy in the coacervate with its higher charge concentration. However, Kudlay and Olvera de la Cruz[11,12] in their theoretical modeling of polyelectrolyte complexation argued that this holds only for hydrophillic polyelectrolytes, for hydrophobic polyelectrolytes, the coacervate is depleted of salt.

Spruijt et al.[7] reported one of the first experimental phase diagrams. They measured coexisting compositions for polyelectrolyte complexes of strongly charged poly(acrylic acid) (PAA) and poly(N,N-dimethylaminoethyl methacrylate) (PDMAEMA) for different molecular weights using fluorescently labeled polymers. They comment that the added salt weakens the cohesion of the coacervate phase and the critical point is observed when the salt concentration is comparable to the concentration of polymeric charges in the complex phase. Following this pioneering work by Spruijt et al., several experimental studies focused on understanding the underlying physics as well as factors affecting the phase behavior[13–16], rheological behavior[17–19], interfacial tension[20,21], chain conformations[22] and critical point[22,23].

The slope of tie lines in a phase diagram reflects the partition of salt between the two phases[9,24–27]. Li et al.[9] studied the phase behavior of coacervates using oppositely charged polypeptides. They report comprehensive phase diagrams, including region near the critical point, showing the effects of salt addition and chain length. They observe a negative slope of tie lines in the phase diagram, indicating a greater salt concentration in the supernatant phase. They also report that "salt resistance", i.e., the excess salt concentration required to produce a single phase, decreases with increasing polymer concentration. Qualitatively similar observations were made by Radhakrishna et al.[24]. in their

[a] Department of Chemical Engineering, The Pennsylvania State University, University Park, Pennsylvania, USA
* E-mail: stm9@psu.edu

Gibbs ensemble Monte Carlo simulations. Zhang et al.[25,26] examined the salt partition in coacervates using thermodynamic analysis of Voorn-Overbeek and liquid state theories. They point out one of the main differences between these two theories to be the opposite sign of the slope of tie line. They attribute this to the Voorn-Overbeek theory ignoring the intrinsic asymmetry in excess chemical potential between polymers and mobile ions that arises due to chain connectivity.

Polymer chain length has only a moderate influence on the coacervate density. Li et al.[9] show that longer polymers form denser complexes and are more resistant towards salt. They argue such trends are expected, as longer polymers have weaker mixing entropy per monomer, leading to larger relative entropy gains from counterion release and thus a stronger propensity for complexation. Spruijt et al.[7] showed that the limiting concentration of polymers in the coacervate phase at very low salt concentrations depends weakly on chain length.

Coacervate phase behavior depends on the choice of added salt[28–31]. Most notably, Schlenoff[31] used different salt ions to show the salt to polymer ratio in the coacervate phase and the partition of salt between the two phases follows the Hofmeister series, which orders ions based on increasing solubility. As we move towards 'hydrophilic' anions (ClO_4^- and I^-), added salt concentration in the coacervate phase was found to be higher than that in the solution. Alternately, ions such as Cl^- and acetate resulted in lower salt concentration in the coacervate phase than in the solution.

The charge density of polyelectrolytes likewise influences the phase behavior. Huang et al.[19] use a large set of polymer combinations prepared by post-polymerization functionalization to show that as the polymer charge density decreases, the salt concentration required to produce a single phase also decreases. Morin et al.[32] developed a method to vary the salt concentration of a coacervate at fixed polymer concentration, by decanting the supernatant and then adding salt directly to the coacervate. In this way, the sample composition moved off the binodal into the single phase region, enabling a study of coacervate viscosity versus added salt.

Recent theoretical approaches have improved on the Voorn-Overbeek theory to model coacervate systems. Qin and de Pablo[33] derive a free energy including mixing entropy, mean-field electrostatic interactions, and fluctuation corrections that depend on molecular architecture. They predict the polymer concentration in the coacervate phase with and without added salt, and find a ternary phase diagram, which varies with charge density and chain length. Additional theoretical advancements include a scaling theory by Rumyantsev et al.[34] for complex coacervates of weakly charged polyelectrolytes that shows the effect of solvent quality and salt concentration. This theory reveals different scaling regimes and boundaries corresponding to crossover between low-high salt concentrations and poor-theta-good solvent conditions. Rubinstein et al.[35] proposed a scaling theory for conformations of polyelectrolytes of different charge densities. They present a phase diagram that shows the impact of salt on such a mixture of unevenly charged polyelectrolytes. Delaney and Fredrickson[36] provide a comparison between the predictions from field theoretic simulations and those from the random phase approximation. Larson et al.[37,38] developed a model to account for charge association-dissociation and pH effects using a closed form free energy expression. This model is used to explain coacervation as a competition between counterion condensation, cross-chain ion-pair formation and charge dissociation. Lou et al.[16] showed that an extension of this model agrees with the experimental observations of oppositely charged polyelectrolytes that have identical structures except for charged groups.

Recently, simulations have been used to predict coacervate phase behavior[24,39–42]. Andreev et al.[39] performed hybrid MC-MD Gibbs ensemble simulations, which reproduce experimental observations on influence of chain length on the phase diagram. In their work, they use a theoretically informed coarse-grained model, parameterized to reproduce the experimental data. Lytle et al.[40] use self consistent field theory (SCFT) and MD simulations to generate the phase diagram and measure interfacial tension. They use a strategy to study the phase boundary, using interfacial density profiles to visualize and obtain the phase diagram. We adapt and extend their strategy in this paper. Similar slab simulations have been previously used to study glassy polymer films[43], polymer-nanoparticle interfaces[44], and the phase behavior of protein assemblies[45].

In this work, we present a simulation model in which all ions, both bonded monomers and mobile counterions, are represented as Lennard-Jones spheres, with a diameter equal to the Bjerrum length and a unit charge on every bead. This choice of diameter avoids Manning condensation[46] in our simulations. That is, it is possible for simulations to represent a large number of counterions that condense into closely associated pairs with oppositely charged ions on chains. Instead, our coarse grained simulations average such effects in terms of effective charges which interact weakly enough that ions do not significantly condense on to the beads. Added salt is modeled as pairs of cation and anion beads, with properties identical to the counterions. We do not include explicit solvent; instead, all beads interact with purely repulsive Lennard-Jones potentials, which corresponds to good solvent conditions.

Without any added salt, the oppositely charged polyelectrolytes with excess solvent form a coacervate phase. The density of this phase is determined by a balance largely between short range repulsion and electrostatic attractions. With addition of salt, we expect the newly added ions to be distributed nearly uniformly through both the coacervate and dilute phases, because in our simulations the electrostatic interaction of each ion in the coacervate is only of the order of kT. Hence added salt swells the coacervate in coexistence with excess solvent, but only by the average volume fraction of mobile ions throughout the system. We expect the total density of chains plus mobile ions in the coacervate to remain roughly constant as salt is added until the critical point, at which the dilute phase and coacervate become identical in composition.

Below, we explore the validity of our physical picture, using molecular dynamics to simulate phase-separated configurations. We obtain a phase diagram using density profiles of polymers and counterions that is qualitatively similar to previous experiments.

We also explore the impact on the phase diagram of increased attractions between polymers as a proxy for changes in solvent quality. Finally, we show that data from experimental phase diagrams exhibit a constant total ion concentration in the coacervate phase, consistent with our physical expectations and simulation results.

2 Methods

In our molecular dynamics simulations, we employ a bead-spring model of oppositely charged chains in which all polymer beads and mobile counterions interact with repulsive Lennard-Jones interactions (eqn. 1)

$$U_{LJ}(r) = \begin{cases} 4\varepsilon((\frac{\sigma}{r})^{12} - (\frac{\sigma}{r})^{6}) + \varepsilon & r \leq r_c \\ 0 & r \geq r_c \end{cases} \quad (1)$$

Here ε = kT (2.49 kJ/mol at 300K). We represent the potential between bonded beads with a stiff harmonic spring, given by:

$$U_{bond}(r) = (1/2)k_b(r - r_0)^2 \quad (2)$$

where, $r_0 = 2^{1/6}\sigma$. We use a spring constant k_b equal to 400 kT/σ^2. Likewise, each bead carries a unit charge, with a Coulomb interaction between beads given by

$$U_{Coul}(r) = kTl_B\frac{z_1 z_2}{r} \quad (3)$$

Here l_B is the Bjerrum length, z_1 and z_2 are the valencies (± 1) and r is the separation distance. We take effective bead diameter $2^{1/6}\sigma$ equal to the Bjerrum length. This choice avoids complications associated with Manning condensation. In effect, we have coarse-grained our system to a scale at which whatever ion condensation would occur, happens at a length scale over which we have averaged. Because of the importance of the coulomb interactions in this system, we use Particle-Mesh Ewald evaluations of coulomb interactions throughout.

We vary the polymer concentration in the simulation box in such a way that the number density of monomer beads is $0.7\phi_p/\sigma^3$, where ϕ_p varies between 0.05 to 0.2. In a two-phase system, the concentration of the polymers in the coacervate will be higher than the average concentration. For reference, charge-neutral polymer melts are represented with a bead concentration of $\phi_m = 0.7/\sigma^3$. In this work, ϕ is the volume fraction relative to ϕ_m.

We simulate oppositely charged polymer chains of length $N = 100$ beads each. Our system consists of 50 polycations and 50 polyanions. We generate initial configurations as random walks near the center of the simulation box. With no added salt, our system includes free counterions equal to the total number of monomers on all the polymers. We add salt by increasing the number of oppositely charged free ion pairs, maintaining charge neutrality.

We start our simulations from a phase-separated configuration. We restrain the polymer center of mass to the center of the simulation box with an umbrella potential with a spring constant of 16 kT/σ^2, in the direction normal to the phase boundary. This potential is sufficient to hold the coacervate phase center of mass to within $\sigma/4$ of the box center. This restraint makes it convenient to visually observe the phase boundary and measure the density profiles of polymers and counterions. This potential is very weak from the point of view of phase behavior and has no effect on the formation or stability of phases. It only acts on the center of mass of all the polymers, which does not cause them to phase separate.

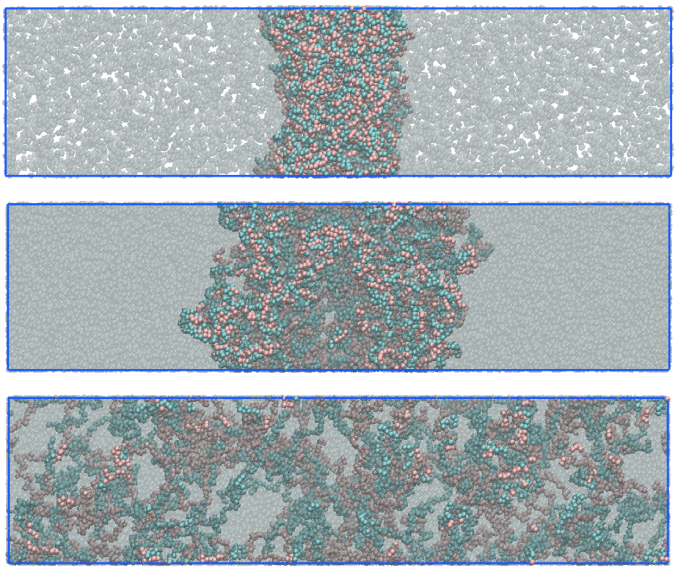

Fig. 1 Simulation snapshots: top, two-phase region with no added salt ($\phi_p = 0.05$); middle, two-phase region with low concentration of added salt ($\phi_{salt} = 0.15$); bottom, one-phase region above the critical point ($\phi_{salt} = 0.5$). Pink and blue beads are polycations and polyanions respectively, free ions are glassy.

For computational efficiency in our bead spring model, we use implicit solvent. That is, we do not include explicit solvent beads. Our polymers and mobile ions move through the apparently empty space. Because of this, the local friction and random forces that would have arisen due to collisions with solvent beads are absent. This makes conventional molecular dynamics problematic, since beads can move only in straight lines between collisions. Hence, we use stochastic dynamics in our simulations in which random forces are added to the velocities of all particles causing them to diffuse even in the empty space.

After an initial energy minimization, we run NVT simulations for 10^8 time steps. Our time step is 0.00228τ, where τ is the Lennard-Jones time $\sigma(m/\varepsilon)^{1/2}$. The phases equilibrate in less than 10^7 time steps. We measure symmetrized density profiles of polymers and counterions over the final 8 x 10^7 time steps, from which we can infer the phase boundary. Correspondingly, the density profile of free ions provides information about the partition of salt between the two phases. We use these density profiles to create a phase diagram and locate the critical point.

3 Results and discussion

Molecular dynamics simulations can effectively reveal the phase behavior of polyelectrolyte complex coacervates. To accomplish this, we equilibrate a slab of polymer-rich coacervate phase in the center of a dilute system of counterions. Adding salt (pairs of counterions) leads to lower concentration of polymer, and higher

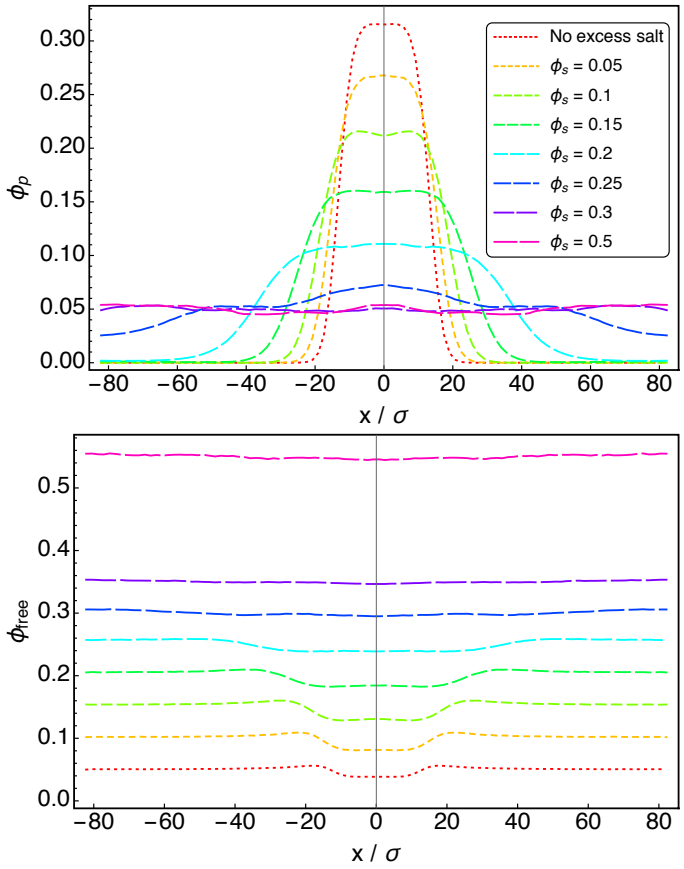

Fig. 2 Density profile of polyelectrolyte chains (top) and counterions (bottom).

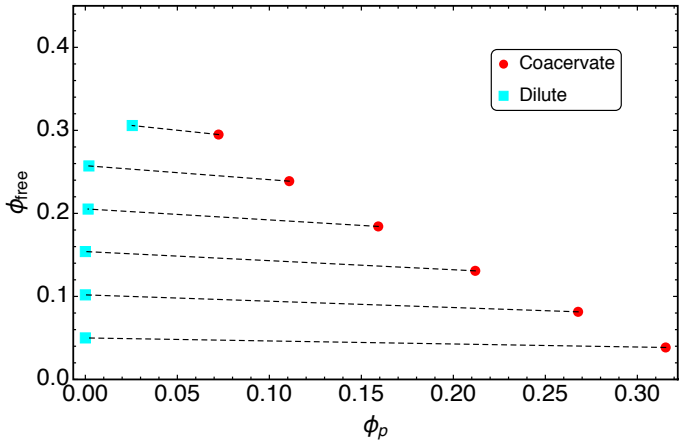

Fig. 3 Coacervate phase diagram. At high enough salt concentration, we observe a one-phase region. Here, the overall polymer volume fraction $\phi_p = 0.05$.

counterion concentration in the coacervate, and thus increased coacervate volume. Adding sufficient salt results in a one-phase liquid (see fig. 1).

Partitioning of polymers and free ions between the phases can be inferred from the density profiles for each species. Because we place the polymer center of mass in an umbrella potential, the coacervate phase appears in the center and the dilute phase at the boundaries. Adding salt swells the coacervate. Except very near the critical point, essentially all the polymers are found in the coacervate phase (see fig. 2 (top)).

Salt is partitioned between the coacervate and the dilute phase. At low salt concentrations, the free ion concentration is slightly higher in the dilute phase. At moderate concentrations of added salt, free ions distribute almost evenly between the two phases. This behavior is evident in fig. 2.

The phase diagram obtained from the density profiles of polymer and free ions (fig. 3) is very asymmetric, with nearly all polymers in the coacervate. The critical point is located near $\phi_p = 0.05$ and $\phi_{free} = 0.3$ (i.e., $\phi_s = 0.25$).

We note in fig. 3 that the total ion concentration in complex phase ($\phi_p + \phi_{free}$) with no added salt is essentially the same as at the critical point. That is, the sum of the ordinate and abcissa of each red data point representing the coacervate phase in fig. 3 is almost the same, equal to about $\phi_{total} \sim 0.35$.

The tie lines have a slightly negative slope, indicating a partitioning of free ions slightly favoring the dilute phase. This observation has been reported in experiments by Li et al.[9] , and in Monte-Carlo based simulations by Radhakrishna et al.[24] and Andreev et al.[39].

Below the critical point, we observe a constant total ion concentration in the coacervate at all polymer and salt concentrations (see fig. 4). This is in agreement with our hypothesis that below the critical point, the coacervate phase can be treated as a liquid of Bjerrum sized ions, whether from polymer or mobile ions. (Above the critical point, the total ion concentration in the single phase evidently equals the system average.)

Spruijt et al.[7] comment on the salt concentration at the critical point. There is a competition between the salt ions and the ionic monomers to form ion pairs. At the critical salt concentration, free ions weaken the cohesion of the complex sufficient for the translational entropy of the polymers to take over. They claim that this happens when the salt concentration is comparable to that of polymeric charges. In our results, we observe a polymer concentration of $\phi_p = 0.32$ in the coacervate phase when there is no additional salt added. We needed to add about $\phi_s = 0.25$ salt to reach the critical point, which is comparable to polymer concentration in the coacervate phase, given that all the monomers on the simulations are charged. Hence, observations from our phase diagram are similar to those from Spruijt's experiments.

For real polymers, the total ion concentration in the coacervate depends on several factors including the chemical structure of monomers, salt, mixing ratio and pH. One way to explore such structural variations in our idealized simulation model is to tune the interactions between the polymers. Until this point, we have assumed purely repulsive Lennard-Jones interactions between all beads. Now, we introduce the attraction between the polymer beads by decreasing σ, while adjusting ε, such that the repulsive strength $\varepsilon\sigma^{12}$ is constant. This increases the attractive strength $\varepsilon\sigma^6$ (see fig. 5).

The coacervate phase becomes denser when attractions are increased between chains. Fig. 6 shows the impact of reducing σ in eqn. 1 to 0.95σ. This small change in σ increases the attractive

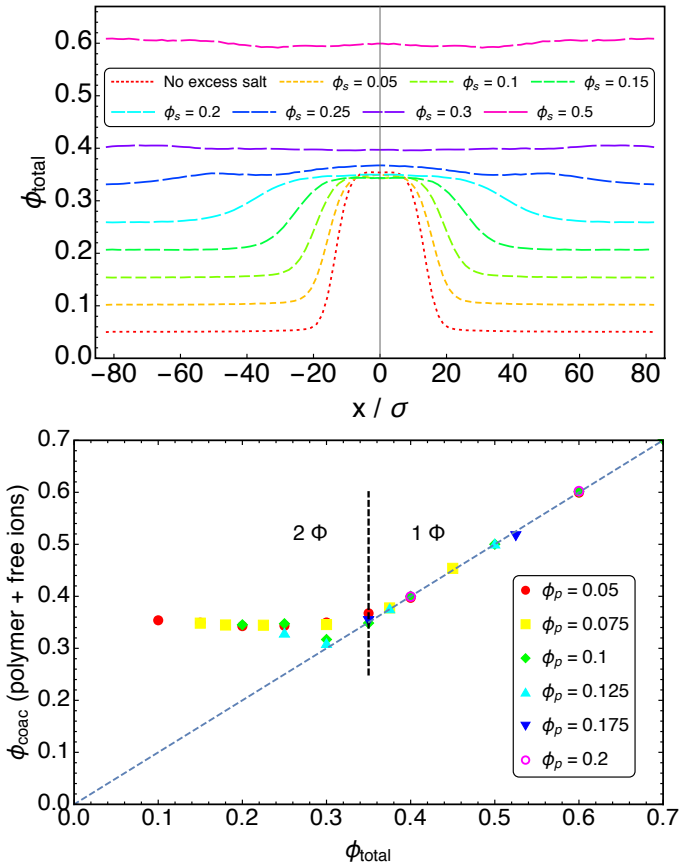

Fig. 4 Overall ion concentration in the coacervate phase remains constant, until the added salt is concentrated enough to produce a single phase. (top) ϕ_{total} at x = 0 is constant in the two phase region for $\phi_p = 0.05$. (bottom) This is observed for a range of total polymer concentrations. Dashed line has slope = 1.

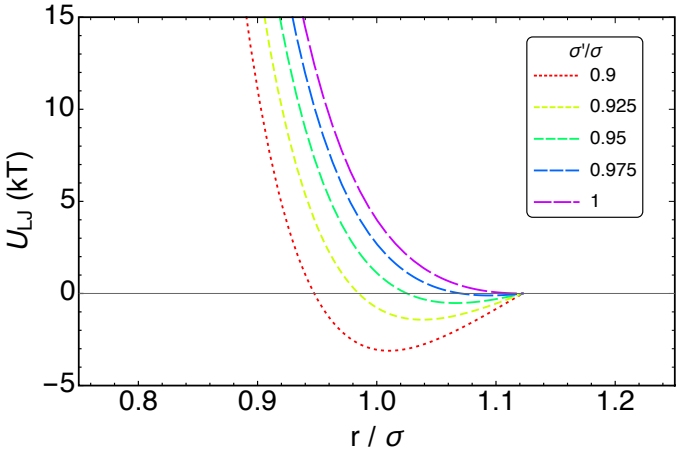

Fig. 5 Polymer-polymer interactions are made more attractive by reducing σ.

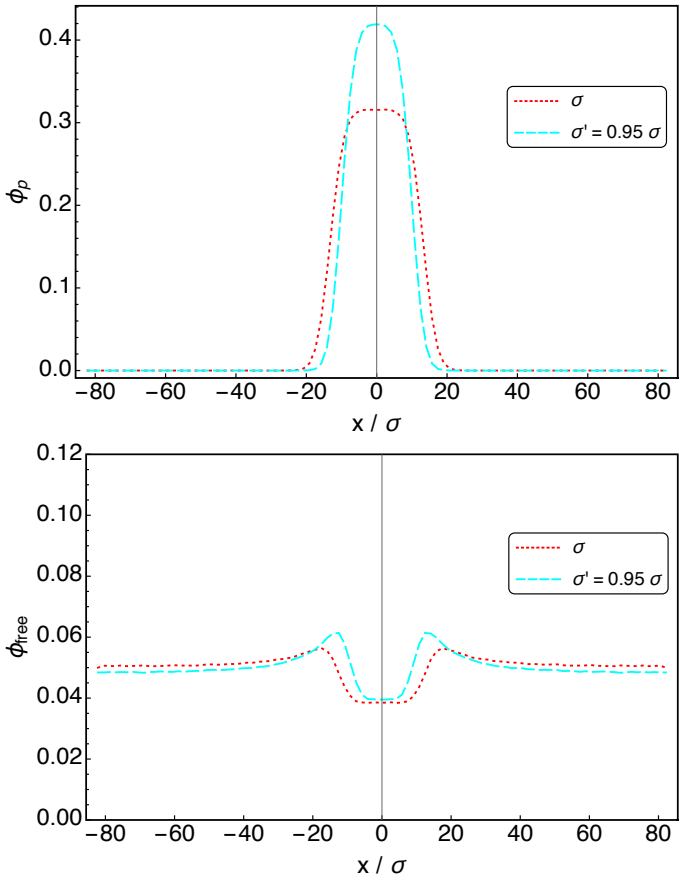

Fig. 6 Polyelectrolytes with increased attractions form a denser coacervate phase as evident from the polymer density profiles (top). The salt partition (bottom) changes only slightly.

term $\varepsilon\sigma^6$ by about 36 percent. Correspondingly, the coacervate phase boundary shifts to higher concentration (see fig. 7). The salt partition is affected only slightly, which is expected since we increased attractions only between polymer beads.

Increased attractions between chains make the complex phase more salt-resistant. Not only is the two-phase region extended to higher concentration, but also the critical point shifts to higher salt concentration in fig. 7.

Even with increased attractions, the ion concentration in the coacervate phase remains constant with addition of salt below the critical point (fig. 8). As expected, this ion concentration for this system is higher than that shown in fig. 4.

We validate our simulation results by comparing them with experimental observations. Here, we are interested in calculating the total ion concentration in the coacervate phase with varying amounts of added salt. We extract data from phase diagrams in the literature from refs. 7,9,32,40, converting reported data into total ion concentration (number of charged ions per unit volume). In our conversions, we assume the polyelectrolytes are completely ionized. Thus the total ion concentration, C^{coac} is sum of charged ions per unit volume on polymers and free ions in the coacervate phase:

$$C^{coac} = \frac{\phi_p^{coac}}{V_{monomer}} + 2\frac{\phi_{salt}^{coac}}{V_{salt}} \quad (4)$$

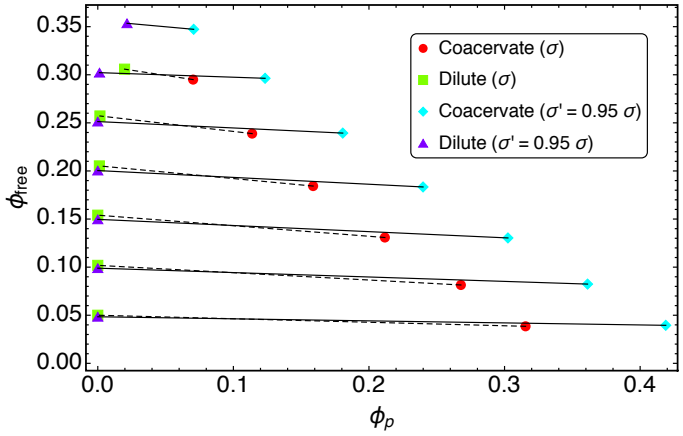

Fig. 7 When attractive forces between polymer beads are increased, the two-phase region broadens, and the coacervate exhibits higher salt resistance. Here, overall polymer volume fraction $\phi_p = 0.05$.

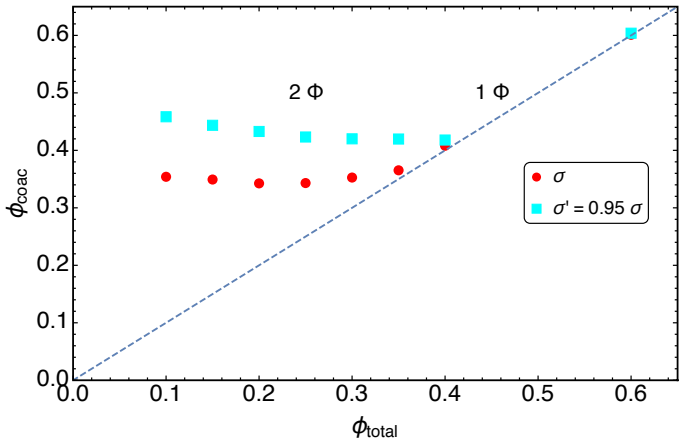

Fig. 8 With increase in attractions between polyelectrolytes, we observe a constant but higher ion concentration in the coacervate phase. Dashed line has slope = 1.

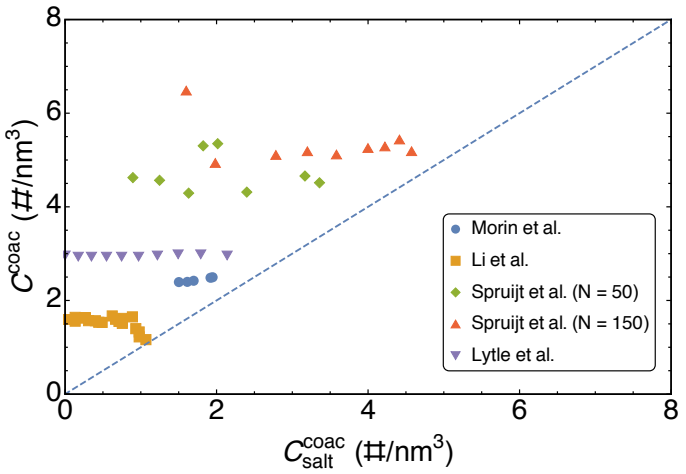

Fig. 9 A compilation of literature data shows that the ion concentration in the coacervate remains constant with addition of salt below the critical point. Dashed line has slope = 1.

Here $V_{monomer}$ and V_{salt} are the molecular volumes of the monomer and salt respectively, ϕ_p^{coac} and ϕ_{salt}^{coac} are the polymer and salt volume fractions in the coacervate. In this expression, the first term is the contribution of ions from the polymers and the second term reflects ions from salt.

We find a constant total ion concentration in the coacervate phase with addition of salt below the critical point in all previous experiments (see fig. 9). The constant value depends on the specific choice of polyelectrolytes and counterions. This striking trend is in agreement with our simulation results (fig. 4).

4 Conclusion

We presented an idealized simulation model for polyelectrolyte complex coacervates. In this bead-spring model all the ions, whether they come from polymers, counterions, or added salt, are represented by beads of unit charge, with diameter equal to the Bjerrum length. This choice avoids counterion condensation as well as long equilibration times associated with binding and unbinding of strongly interacting ions. Salt is represented by pairs of oppositely charged ions. We do not explicitly include solvent, but instead represent good solvent conditions with purely repulsive Lennard-Jones potential.

We started our simulations with a slab of concentrated coacervate phase in the center and free counterions evenly distributed in the simulation box. With no added salt, the oppositely charged chains are well mixed in the coacervate phase and the dilute phase is depleted of polymers. We observed a distinct phase boundary between the two phases.

We used the density profiles of polymers and free ions to construct the phase diagram. At low added salt concentrations, we observed a small negative slope for the tie lines connecting the concentrations in the two phases. This indicates a slight preference of free ions towards the dilute phase.

The coacervate phase swells with addition of salt, but only by the average volume fraction of the mobile ions. Added salt distributes uniformly, because intimately mixed and oppositely charged chains do not provide particularly favorable sites for the

incoming mobile ions, and the electrostatic interactions of near-neighbor pairs are only of order kT. This implies that the total ion concentration in the coacervate phase remains constant for the two phase system, as observed in fig. 4.

In other words, the coacervate phase at all polymer concentrations, consists of an ionic solution at roughly the critical salt concentration. In terms of our bead-spring model, the coacervate phase is always a dense liquid of Bjerrum length sized ions, which may either be from polymers or from the mobile ions. We find the same behavior in data extracted from published experimental phase diagrams.

To investigate effects of solvent quality on coacervate phase behavior, we introduced modest attractions between polymer beads. Increased attractions led to formation of denser coacervates, and the critical point was found at higher salt concentration. This finding suggests that hydrophobic effects may explain the variation of salt resistance of real coacervates in which polymers with large hydrophobic segments would qualitatively correspond to our systems in which there is more attraction between beads.

Acknowledgements

The authors acknowledge financial support from NSF under DMR-1905632.

Notes and references

1 K. A. Black, D. Priftis, S. L. Perry, J. Yip, W. Y. Byun and M. Tirrell, *ACS Macro Letters*, 2014, **3**, 1088–1091.

2 A. C. Obermeyer, C. E. Mills, X.-H. Dong, R. J. Flores and B. D. Olsen, *Soft Matter*, 2016, **12**, 3570–3581.

3 Q. Zhao, D. W. Lee, B. K. Ahn, S. Seo, Y. Kaufman, J. N. Israelachvili and J. H. Waite, *Nature materials*, 2016, **15**, 407–412.

4 S. Turgeon, C. Schmitt and C. Sanchez, *Current Opinion in Colloid & Interface Science*, 2007, **12**, 166–178.

5 C. Schmitt and S. L. Turgeon, *Advances in colloid and interface science*, 2011, **167**, 63–70.

6 C. E. Sing and S. L. Perry, *Soft Matter*, 2020, **16**, 2885–2914.

7 E. Spruijt, A. H. Westphal, J. W. Borst, M. A. Cohen Stuart and J. van der Gucht, *Macromolecules*, 2010, **43**, 6476–6484.

8 J. Van der Gucht, E. Spruijt, M. Lemmers and M. A. Cohen Stuart, *Journal of colloid and interface science*, 2011, **361**, 407–422.

9 L. Li, S. Srivastava, M. Andreev, A. B. Marciel, J. J. de Pablo and M. V. Tirrell, *Macromolecules*, 2018, **51**, 2988–2995.

10 J. T. G. Overbeek and M. J. Voorn, *Journal of Cellular and Comparative Physiology*, 1957, **49**, 7–26.

11 A. Kudlay and M. Olvera de la Cruz, *The Journal of chemical physics*, 2004, **120**, 404–412.

12 A. Kudlay, A. V. Ermoshkin and M. Olvera de La Cruz, *Macromolecules*, 2004, **37**, 9231–9241.

13 D. Priftis, N. Laugel and M. Tirrell, *Langmuir*, 2012, **28**, 15947–15957.

14 S. L. Perry, L. Leon, K. Q. Hoffmann, M. J. Kade, D. Priftis, K. A. Black, D. Wong, R. A. Klein, C. F. Pierce, K. O. Margossian *et al.*, *Nature Communications*, 2015, **6**, 1–8.

15 D. Priftis, X. Xia, K. O. Margossian, S. L. Perry, L. Leon, J. Qin, J. J. de Pablo and M. Tirrell, *Macromolecules*, 2014, **47**, 3076–3085.

16 J. Lou, S. Friedowitz, J. Qin and Y. Xia, *ACS central science*, 2019, **5**, 549–557.

17 E. Spruijt, J. Sprakel, M. Lemmers, M. A. Cohen Stuart and J. Van Der Gucht, *Physical review letters*, 2010, **105**, 208301.

18 E. Spruijt, M. A. Cohen Stuart and J. van der Gucht, *Macromolecules*, 2013, **46**, 1633–1641.

19 J. Huang, F. J. Morin and J. E. Laaser, *Macromolecules*, 2019, **52**, 4957–4967.

20 E. Spruijt, J. Sprakel, M. A. Cohen Stuart and J. van der Gucht, *Soft Matter*, 2010, **6**, 172–178.

21 J. Qin, D. Priftis, R. Farina, S. L. Perry, L. Leon, J. Whitmer, K. Hoffmann, M. Tirrell and J. J. De Pablo, *ACS Macro Letters*, 2014, **3**, 565–568.

22 S. Xie, B. Zhang, Y. Mao, L. He, K. Hong, F. S. Bates and T. P. Lodge, *Macromolecules*, 2020, **53**, 7141–7149.

23 R. Chollakup, J. B. Beck, K. Dirnberger, M. Tirrell and C. D. Eisenbach, *Macromolecules*, 2013, **46**, 2376–2390.

24 M. Radhakrishna, K. Basu, Y. Liu, R. Shamsi, S. L. Perry and C. E. Sing, *Macromolecules*, 2017, **50**, 3030–3037.

25 P. Zhang, N. M. Alsaifi, J. Wu and Z.-G. Wang, *The Journal of chemical physics*, 2018, **149**, 163303.

26 P. Zhang, K. Shen, N. M. Alsaifi and Z.-G. Wang, *Macromolecules*, 2018, **51**, 5586–5593.

27 M. Ghasemi, S. Friedowitz and R. G. Larson, *Macromolecules*, 2020, **53**, 6928–6945.

28 K. Sadman, Q. Wang, Y. Chen, B. Keshavarz, Z. Jiang and K. R. Shull, *Macromolecules*, 2017, **50**, 9417–9426.

29 P. K. Jha, P. S. Desai, J. Li and R. G. Larson, *Polymers*, 2014, **6**, 1414–1436.

30 S. L. Perry, Y. Li, D. Priftis, L. Leon and M. Tirrell, *Polymers*, 2014, **6**, 1756–1772.

31 J. B. Schlenoff, M. Yang, Z. A. Digby and Q. Wang, *Macromolecules*, 2019, **52**, 9149–9159.

32 F. J. Morin, M. L. Puppo and J. Laaser, *Soft Matter*, 2021, **17**, 1223–1231.

33 J. Qin and J. J. de Pablo, *Macromolecules*, 2016, **49**, 8789–8800.

34 A. M. Rumyantsev, E. B. Zhulina and O. V. Borisov, *Macromolecules*, 2018, **51**, 3788–3801.

35 M. Rubinstein, Q. Liao and S. Panyukov, *Macromolecules*, 2018, **51**, 9572–9588.

36 K. T. Delaney and G. H. Fredrickson, *The Journal of chemical physics*, 2017, **146**, 224902.

37 A. Salehi and R. G. Larson, *Macromolecules*, 2016, **49**, 9706–9719.

38 S. Friedowitz, A. Salehi, R. G. Larson and J. Qin, *The Journal of chemical physics*, 2018, **149**, 163335.

39 M. Andreev, V. M. Prabhu, J. F. Douglas, M. Tirrell and J. J. de Pablo, *Macromolecules*, 2018, **51**, 6717–6723.

40 T. K. Lytle, A. J. Salazar and C. E. Sing, *The Journal of chemical*

physics, 2018, **149**, 163315.

41 R. A. Riggleman, R. Kumar and G. H. Fredrickson, *The Journal of chemical physics*, 2012, **136**, 024903.

42 B. Peng and M. Muthukumar, *The Journal of chemical physics*, 2015, **143**, 243133.

43 S. Neyertz and D. Brown, *Computational Materials Science*, 2020, **174**, 109499.

44 S. Chakraborty, F. C. Lim and J. Ye, *The Journal of Physical Chemistry C*, 2019, **123**, 23995–24006.

45 G. L. Dignon, W. Zheng, R. B. Best, Y. C. Kim and J. Mittal, *Proceedings of the National Academy of Sciences*, 2018, **115**, 9929–9934.

46 G. S. Manning, *The journal of chemical Physics*, 1969, **51**, 924–933.